Desalination and Water Treatment
www.deswater.com

doi: 10.5004/dwt.2019.24729

169 (2019) 88–101
November

Assessment of a double slope solar still for the distillation of cenote water in the Yucatan peninsula – thermal and economic analysis

J. Gual-Uc[a], J.G. Carrillo[a,*], A. Bassam[b], M. Flota-Bañuelos[b], C.A. Pineda-Arellano[c]

[a]*Unidad de Materiales, Centro de Investigacion Cientifica de Yucatan, A.C., C. 43, No. 130, Chuburna de Hgo. 97205, Merida, Mexico, emails: jgcb@cicy.mx (J.G. Carrillo), jonathan.gual@hotmail.com (J. Gual-Uc)*
[b]*Facultad de Ingenieria, Universidad Autonoma de Yucatan, Av. Industrias no contaminates, Apdo. Postal 150, Merida, Mexico, emails: baali@correo.uady.mx (A. Bassam), manuel.flota@correo.uady.mx (M. Flota-Bañuelos)*
[c]*CONACYT – Centro de Investigaciones en Optica, A.C., Unidad Aguascalientes, Prol. Constitucion 607, Fracc. Reserva Loma Bonita, CP 20200, Aguascalientes, Mexico, email: capia@cio.mx*

Received 23 February 2019; Accepted 24 July 2019

ABSTRACT

The urban population of the Yucatan peninsula in Mexico is experiencing water shortages; in consequence, they are obliged to use the unclean water from surrounding cenotes. In this work, an analysis for the distillation of the cenote water is conducted, using a solar still. The novelty of this work is that it can provide a solution which will ensure safe drinking water for the residents of Yucatan in a sustainable manner. For this purpose, a double slope solar still has been developed and its performance for the climatic region of Yucatan is presented for one complete year, with the purpose of determining its capacity of disinfection, productivity and efficiency. The yearly averaged production resulted was 3.44 L/(m^2 d). The yearly, monthly and daily thermal performance is presented in terms of operating temperatures of the solar still, heat flux, water production rate, internal and instantaneous efficiency. The quality of the water was measured before and after the distillation process, attaining a purity of 99% as per the standards of the World Health Organization. The financial analysis has shown an attractive investment recovery of 1.8 years.

Keywords: Solar still; Energy analysis; Solar orientation; Basin water depth; Distillation; Efficiency

1. Introduction

The lack of access to drinking water, its quality and consistent availability are just a few of the main problems affecting the world at present. A large part of the rural areas in developing countries, such as Mexico, do not have access to drinking water due to population dispersion, physiographic conditions, technical and financial problems; thus, making it is difficult to install infrastructure in these areas. The large urbanized cities are the main consumers of water; therefore, the priority of the Mexican government is the water needs in those areas; thus, neglecting the more vulnerable rural population. In addition, the irrational use of water and its scarcity, together with an increase in the population, has made it necessary for the inhabitants of the rural areas to use the water from aquifers, rainfall, rivers or lakes without any type of treatment. Moreover, the anthropogenic activities of the urban areas have caused a higher level of water contamination in the fresh water resources; thus, the provision of drinkable water is more difficult for rural population.

The Yucatan peninsula of Mexico also experiences the water scarcity because of ineffective distribution of drinkable water in such a high population density region. One possible alternative for this region of Mexico is to utilize the

* Corresponding author.

1944-3994/1944-3986 © 2019 Desalination Publications. All rights reserved.

water from the cenotes (Fig. 1) which is a natural water well formed from the collapse of limestone bedrock that exposes groundwater underneath. It is estimated that the Yucatan peninsula alone, contains more than 6,000 [1] cenotes, where some others remain undiscovered. A list of a few public cenotes in the Yucatan region is presented in Fig. 1a. Most of the time, the water in the cenotes is density-stratified because the infiltrating rain water remains on the top of the high-density saline water. This interface of saline and fresh water, called halocline, presents a very sharp change in the concentration of the salt according to its depth. Therefore, the cenote water must be subjected to a desalination process before being used for drinking purposes. Based on morphometry-based classification, a cenote has four categories. The pit type cenote has a narrower surface connection in comparison with the diameter of the water body, the cylinder type cenote has vertical walls, the basin type cenote has a shallow water basin and the cave type cenote has a horizontal entrance with a dry section. A photograph of the shallow water basin type cenote is presented in Fig. 1b.

At present, different processes are available for the treatment of saline water collected from Yucatan cenotes, such as filtration by active carbon which eliminates dissolved and undissolved particles, but not certain bacteria; humidification dehumidificationdesalination [2] which is only economical for a higher fresh water productivity rate, ultraviolet rays which eliminate the pathogenic agents, but not the dissolved and undissolved particles; inverse osmosis and electrodialysis which need electric power and are applicable in urbanized settlements, but limited and expensive for remote areas [3]. Therefore, many researchers in worldwide agree that one of the best alternative for treating brackish water in remote areas is solar distillation, since it eliminates pathogenic agents as well as dissolved and undissolved particles, providing an immediate, simple and economic method to obtain drinking water from solar thermal energy. Although a number of studies have been conducted on solar distillation, the low productivity of these systems has made their applications somewhat limited and at present many studies are focusing on the development of more efficient and viable devices with competitive costs for applications on a large scale [4].

The solar still subjects the water to a process of evaporation and condensation, after which it is free of contaminating agents, without generating pollution in the environment [6]. Upon further classifications of the solar still, Sivakumar and Ganapathy Sundaram [7] proposed that a passive solar still is more economical because of its lower manufacturing, operational and maintenance cost. Additionally, among the many other structural configurations of the solar still including single slope [8], double slope [9–12], tubular [13], cascade type [14] and hemispheric type [15], Rajamanickam and Ragupathy [16] carried out a comparative study between a single slope and a double slope solar still, having similar dimensional, material and operating parameters. Their results have indicated that the production rate for the single slope is 2.34 L/(m^2 d) and for the double slope this is 3.07 L/(m^2 d); thus, the latter provides a better yield given the versatility in its spatial orientation. Several other authors carried out the analysis of a solar still for different climatic conditions. Abdessemed et al. [17] evaluated the performance of a hybrid solar still working with different types of energy sources in Argelia. Yousef et al. [18] analyzed a single slope solar still based on energy and exergy analysis for the climatic conditions of Egypt. Similarly, Tiwari and Somwanshi [19] carried out the analysis for India and Mashaly and Alazba [20] analyzing the solar still for arid climatic regions. Additionally, water depth is an important factor to consider when designing a solar still. Some researchers have been evaluating the correspondence of water depth and its efficiency on distilling water at different water depths; results show in all studies that low depth water at the basin gains temperature faster and speeds up the evaporation process, making the system more efficient [21–24].

Previous states-of-the-art has shown that no research has been carried out on the source of cenote water, and specifically no such work has been carried out for the region of Yucatan, Mexico, with the aim of obtaining clean water in rural areas. The main objective of this work is to present a solution for the people living in the Yucatan peninsula to desalinate and disinfect the water from the cenote and to use it for drinking purposes. This research plays an important

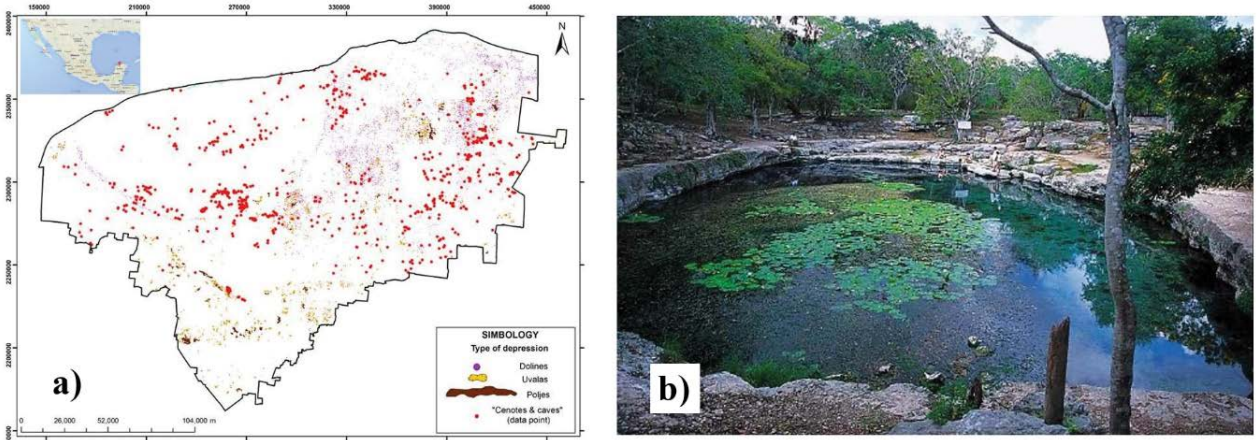

Fig. 1. (a) Map of Yucatan, Mexico showing the locations of the cenotes and (b) photograph of a shallow water basin type cenote located in the state of Yucatan, Mexico [5].

role in the state-of-the-art literature given that it addresses an important issue in the problem relating to the drinking water, especially for the small communities disperse in Yucatan region. For this purpose, the authors have developed an experimental setup of a solar still for the distillation of the cenote water collected from the Sisbichen community in Yucatan, Mexico. Furthermore, the prime novelty of this work is to study the performance of the solar still for the climatic conditions of Yucatan using the cenote water of the study site. Therefore, in this work, the authors presented an experimental analysis on the most suitable orientation for the solar still, and the influence of the water depth on its performance. The authors have also presented the performance of the solar still on daily, monthly and yearly basis. Quality analysis of the cenote water is also carried out before and after the distillation process, and finally the authors have presented the financial analysis of the solar still.

2. System description

The double slope solar still is constructed and evaluated in the city of Merida, Yucatan, Mexico (latitude: 20° 58′ N, longitude: 89° 37′ O), with a tropical savanna climate having the presence of rainfall between the months of June and October and an annual average temperature of 26°C. The prototype is fabricated to produce 1 L of water per day which has an effective area of 0.4 m^2, considering the environmental parameters such as solar irradiance, wind speed and ambient temperature.

The details of the construction are shown in Fig. 2a. The glass cover of the solar still which acts as a condenser has a thickness of 3 mm and its slope is equal to the latitude of the operational site, which in this case is 21°. The solar collector and the evaporator are fabricated with the aluminum basin having dimensions of 0.72 m^3 × 0.43 m^3 × 0.035 m^3 and a thickness of 1 mm, located at the bottom of the system. A detachable lid is used for maintenance as well as for the introduction and removal of the basin from the solar still. An extruded 10 mm polystyrene laminate is located under the solar collector and its thickness is calculated using Fourier's conductive heat transfer law. For the body of the solar still, 6 mm acrylic sheet is used, given its reliable mechanical and thermal characteristics, in comparison with conventional glass; furthermore, handling of the acrylic sheet is also easier than conventional glass (cutting, bonding and screwing parts). The channels for water collection are also made of acrylic sheets and are attached to the lateral walls of the solar still maintaining a slope of 2°. The distilled water outlet is connected to a storage tank (3 L capacity) using a flexible hose. An external brackish water tank with a capacity of 5 L is connected to a sealed pipeline system which is able to provide a dosage and vary the height of the water level (by gravity) in the basin. This supplied a constant flow rate of brackish water, and by interchanging the tube tip, it was possible to control the water height as required (1 cm, 2 cm and 3 cm).

Fig. 2b shows the dimensions of the solar still which are: longitude = 0.75 m, width = 0.50 m and height = 0.158 m, the supporting structure has a height of 0.5 m, and the effective area is 0.40 m^2 for the glass cover and basin. The maximum height of the lateral walls of the solar still is 6.5 cm and, by means of simple trigonometry, the dimensions of the glass cover and the height of the air chamber are determined.

In order to obtain the temperature data in different parts of the system, six digital sensors DS18B20 were installed; one in the basin (S1), two immersed in the water (S2 and S3), one in each glass cover (S4 and S5) and one ambient temperature reference (S6) connected to a microcontroller managed by a remote computer program.

Fig. 3 presents the experimental setup of the solar still in use, where sediments of the lime scale can be observed during its working operation, which is an outcome of the distillation process.

3. Mathematical modelling

The energy exchange in the system occurs in following modes: by conduction through its physical components, by convection between the water vapor and the interior surface of the glass covers (also by wind movement on the exterior surface), by radiation between its surfaces due to temperature difference, and also because of the conjugate heat and

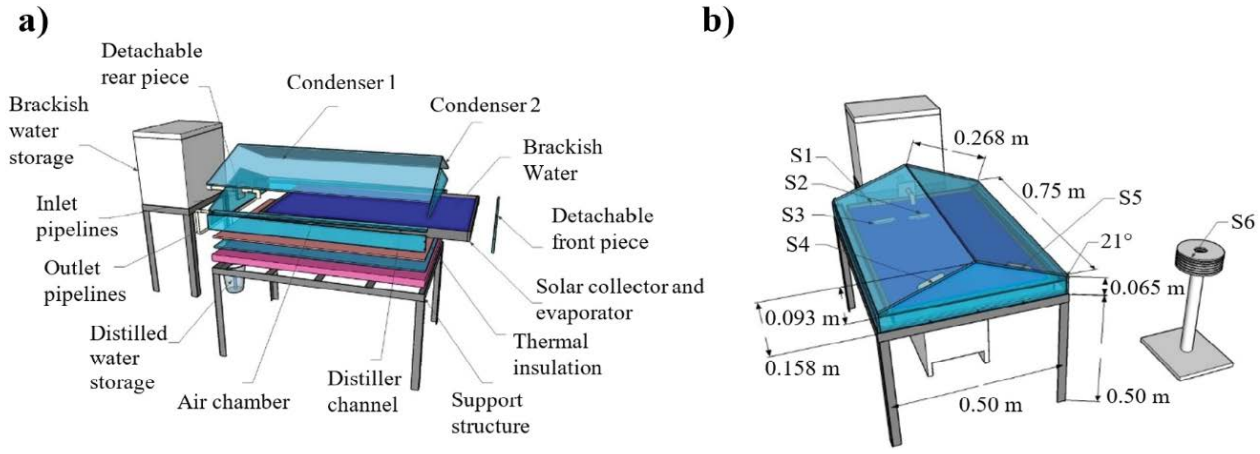

Fig. 2. Double slope solar still, (a) elements in its structure with consideration in its design and (b) dimensions and distribution of the temperature sensors.

Fig. 3. Experimental setup of double slope solar still.

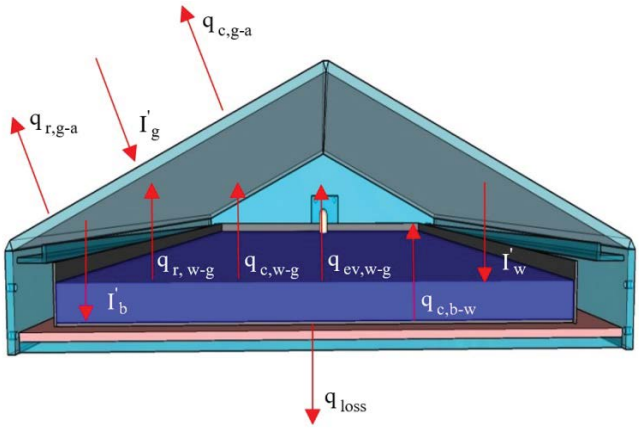

Fig. 4. Transverse section view of the still configuration and mechanisms of heat and mass transfer, which govern its functioning.

mass transfer phenomena during evaporation–condensation. An analytical study is presented to calculate the efficiency based on heat and mass transfer equations for this type of solar energy systems (Fig. 4).

The radiative heat transfer from the glass covers to the ambient air is defined by the following expression [25]:

$$q_{r,g-a} = h_{r,g-a}\left(T_g - T_a\right) \tag{1}$$

The radiative heat transfer coefficient between the glass covers and the ambient air is expressed as:

$$h_{r,g-a} = \varepsilon_g \sigma \left[\frac{\left(T_g + 273.15\right)^4 - \left(T_s + 273.15\right)^4}{T_g - T_a}\right] \tag{2}$$

The temperature of the sky appearing in Eq. (2) is calculated using:

$$T_s = T_a - 6 \tag{3}$$

Heat transfer by convection between the glass covers and the ambient air is calculated using [26]:

$$q_{c,g-a} = h_{c,g-a}\left(T_g - T_a\right) \tag{4}$$

The convective heat transfer coefficient from the glass covers to the ambient air is dependent on wind speed expressed as:

$$h_{c,g-a} = \begin{bmatrix} 2.8 + 3v \text{ if } v \le 5 \text{ m/s} \\ 6.15v^{0.8} \text{ if } v \ge 5 \text{ m/s} \end{bmatrix} \tag{5}$$

Heat transfer by radiation between the water and the glass covers is defined as follows [27]:

$$q_{r,w-g} = h_{r,w-g}\left(T_w - T_g\right) \tag{6}$$

The convective heat transfer coefficient between the glass covers and the water is defined as:

$$h_{r,w-g} = \varepsilon_{\text{eff},w-g}\sigma\left[\left(T_w + 273.15\right)^4 + \left(T_g + 273.15\right)^4\right]\left(T_w + T_g + 546.3\right) \tag{7}$$

where the effective emissivity between the water and the glass covers is expressed by:

$$\varepsilon_{\text{eff},w-g} = \left(\frac{1}{\varepsilon_w} + \frac{1}{\varepsilon_g} - 1\right)^{-1} \tag{8}$$

Heat transfer by convection from the surface of the water to the glass covers is defined as:

$$q_{c,w-g} = h_{c,w-g}\left(T_w - T_g\right) \tag{9}$$

where the coefficient of heat transfer by convection from the water to the glass covers is given by:

$$h_{c,w-g} = 0.884\left(\left(T_w - T_g\right) + \frac{\left(P_w - P_g\right)\left(T_w + 273.15\right)}{268.9 \times 10^3 - P_w}\right)^{1/3} \tag{10}$$

The saturation pressure for T values in a range of 10°C–90°C can be calculated by the following expression:

$$P\left(T\right) = \exp\left[25.317 - \left(\frac{5144}{T + 273.15}\right)\right] \tag{11}$$

Heat transfer by water evaporation is shown in the following equation [13]:

$$q_{\text{ev},w-g} = h_{\text{ev},w-g}\left(T_w - T_g\right) \tag{12}$$

where the evaporative heat transfer coefficient of the water is represented as:

$$h_{\text{ev},w-g} = 16.273 \times 10^{-3}\left[h_{c,w-g}\left(\frac{P_w - P_g}{T_w - T_g}\right)\right] \tag{13}$$

Heat transfer by convection between the basin and the water is defined as [28]:

$$q_{c,b-w} = h_{c,b-w}\left(T_b - T_w\right) \tag{14}$$

where the convective heat transfer coefficient from the basin to the water is represented as:

$$h_{c,b-w} = \begin{bmatrix} 0.54\dfrac{k_w \mathrm{Ra}_w^{1/4}}{L_w} \text{ if } 10^4 < \mathrm{Ra} < 10^7 \\ 0.15\dfrac{k_w \mathrm{Ra}_w^{1/3}}{L_w} \text{ if } 10^7 < \mathrm{Ra} < 10^{11} \end{bmatrix} \tag{15}$$

The overall heat loss in the base of the solar still is primarily by conduction from the basin to the insulation and by convection and radiation from the insulation to the ambient air and is defined as follows [29]:

$$q_{\mathrm{loss}} = U_b\left(T_b - T_a\right) \tag{16}$$

where the overall heat loss coefficient in the solar still is written as:

$$U_b = \left(\frac{\delta_b}{k_b} + \frac{\delta_i}{k_i} + \frac{1}{h_{c,b-w}}\right)^{-1} \tag{17}$$

The fraction of solar energy directly absorbed by the glass covers, the water and the basin are shown in the following expressions [30]:

$$I'_g = \left(1-\rho_g\right)\alpha_g I_T \tag{18}$$

$$I'_w = \left(1-\alpha_g\right)\left(1-\rho_g\right)\left(1-\rho_w\right)\alpha_w I_T \tag{19}$$

$$I'_b = \left(1-\alpha_g\right)\left(1-\rho_g\right)\left(1-\rho_w\right)\left(1-\alpha_w\right)\alpha_b I_T \tag{20}$$

The energy balance equation on the glass cover can be written as:

$$q'_v = q_{r,w-g} + q_{c,w-g} + q_{\mathrm{ev},w-g} + I'_g - \left(q_{r,g-a} + q_{c,g-a}\right) \tag{21}$$

The energy balance on the water is shown as:

$$q'_w = I'_w + q_{c,b-w} - \left(q_{r,w-g} + q_{c,w-g} + q_{\mathrm{ev},w-g}\right) \tag{22}$$

The energy balance on the basin is shown as follows:

$$q'_b = I'_b - \left(q_{c,b-w} + q_{\mathrm{loss}}\right) \tag{23}$$

The total energy balance on the system can be determined by the summation of all the individual energy balance on the glass cover, water and the basin which is given by:

$$q'_T = q'_v + q'_w + q'_b \tag{24}$$

The internal thermal efficiency of the solar still is defined as the relationship between the quantity of energy used by the system and the available solar energy:

$$\eta_{\mathrm{int}} = \frac{q'_T}{I_T} \times 100 \tag{25}$$

The instantaneous efficiency of the system is represented as the evaporation speed of a certain amount of mass with respect to the quantity of solar energy in the determined period of time [25]:

$$\eta_{\mathrm{ins}} = \frac{q_{\mathrm{ev}}}{I_T} \times 100 \tag{26}$$

The quantity of distilled water per hour can be estimated as [25]:

$$m_{\mathrm{ev}} = h_{\mathrm{ev},w-g}\frac{\left(T_w - T_g\right)}{\lambda_w} \times 3600 \tag{27}$$

4. Results and discussion

4.1. Orientation selection for the solar still in the region of Merida, Mexico

In this section, experiments are carried out to find the most suitable orientation for the solar still in the region of Merida, Mexico. For this purpose, experiments are carried out for two orientations namely North-South orientation, and East-West orientation. Fig. 5 shows the thermal evaluation for the North-South (Fig. 5a) and East-West orientations (Fig. 5b); in 2 d with similar climate conditions (solar irradiance: 750 W/m^2, wind speed: 2 m/s, relative humidity: 77%, dew point: 22.5°C, ambient temperature: 30°C). The results obtained in this analysis show a clear difference in the thermal behavior of the system and consequently in the fresh water productivity for the said location.

It can be observed from Fig. 5a that at the beginning of the day, both glass covers present a similar increase in temperature in accordance with the increasing solar irradiance. However; between 800 and 1,200 h the south glass cover, which initially receives the solar energy, experiences a slight warming of around 0.68°C, in comparison with the north glass cover. As the time advances, by 1,400 h both glass covers have reached their highest temperatures, differing by approximately 0.35°C (57.75°C north glass and 57.40°C south glass). Some hours later, the north glass cover experiences a slight dominance of approximately 0.40°C due to the direction of incident solar irradiance in the afternoon, caused by the effects of the accumulated heat in the solar still and by the predominant direction of the wind on the south glass cover. The average daytime temperature of the north and south glass covers is 48.36°C and 48.27°C respectively, representing a minimal difference of approximately 0.08°C. In other words, besides the trajectory of the sun, no important asymmetries were presented in the thermal behavior of the glass covers during the day, where the effects of the wind provoked small thermal differences. For this orientation, with the transmission effects of the solar irradiance through

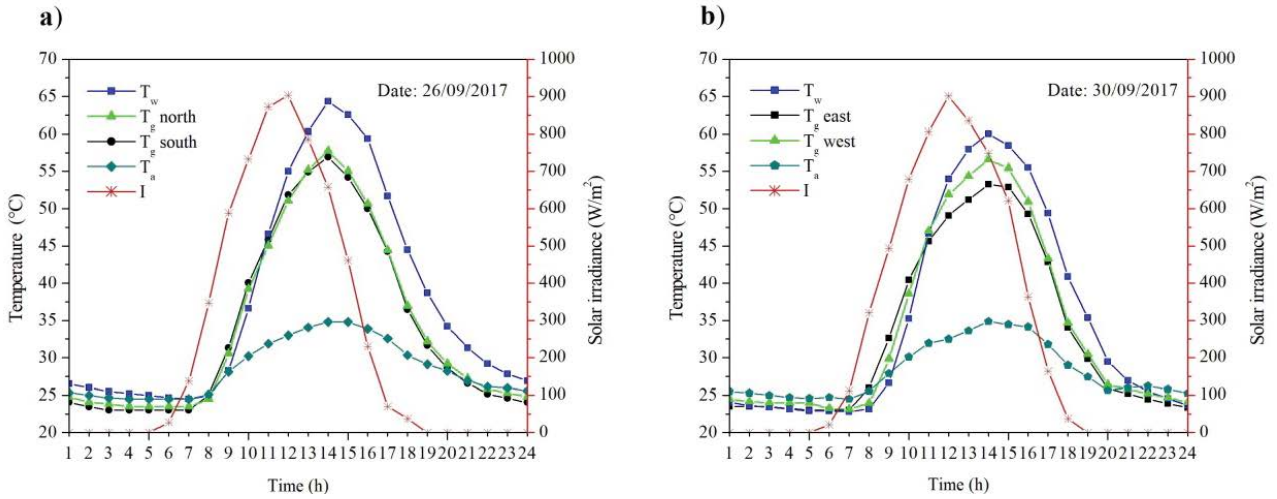

Fig. 5. Thermal characteristics in the solar still for (a) North-South orientation and (b) East-West orientation.

the glass covers, an average daytime temperature of 53.44°C was obtained for the water, where the difference with the average temperature of the glass covers is 5.12°C.

Fig. 5b shows the temperatures obtained for the East-West orientation and, in this case, between 700 h and 1,000 h, the East glass cover was subjected to an early warming of approximately 1.7°C in comparison with the West cover; because the East face is oriented favorably towards the rising sun. At 1,400 h, both glass covers had reached their highest temperatures for the East and West glass covers; 53.25°C and 56.58°C respectively, differing by 3.33°C. This is because the incident radiation in the afternoon is facing the West glass cover and in addition, the wind direction is dominant towards the East glass cover; thus, lowering its temperature in comparison with the West glass cover. The average daytime temperatures for the East and West glass covers are 47.18°C and 49.25°C, respectively, differing in 2.07°C. It is reported that higher asymmetries are observed in the thermal behavior of both glass covers; a consequence of being exposed to the sun at different times of the day. However, the role of wind direction is important in causing this asymmetry in the glass cover temperature. Moreover, these asymmetries are more dominant after midday. For this orientation, due to the effects of solar irradiance transmission through the glass covers, an average daytime temperature of 51.13°C is obtained for the water and its difference with the average glass temperature is 2.91°C.

Although a reasonable temperature difference can be observed for both orientations, and the North-South orientation attains the highest temperature curves; the analysis based on water productivity rate must be carried out to clearly present the difference in performance for both orientations. For this purpose, the distillate production rate is calculated for both of the orientations and the results are presented in Fig. 6. Fig. 6a presents the thermal behavior for the North-South orientation and one can observe that its performance is similar for both glass covers. In this case, both of the glass covers are exposed to the same solar radiation; therefore, similar glass cover temperatures are observed (Fig. 6a); thus causing a similar yield of 0.90 and 0.95 L/d for both glass covers, with a difference of only 5%. Considering this, the total yield of fresh water for North-South orientation is 1.85 L/d. The thermal behavior of the glass covers for the East-West orientation (Fig. 6b) is quite asymmetric given that the East glass cover experiences a quick temperature change in comparison with that of the West glass cover; thus, it provokes a significant change in their fresh water production rate. The distillate production rate is 0.87 L/d (East glass) and 0.71 L/d (West glass), a total of 1.58 L/d for both glass covers (Fig. 6b); thus, differing from each other by 18%.

In conclusion, from this section, the comparative analysis for both orientations have shown that the smaller thermal asymmetries are observed for the North-South orientation and higher thermal asymmetries are observed for the East-West orientation. Furthermore, the fresh water production rate for the North-South orientation is 14% higher in comparison with the East-West orientation; therefore the use the North-South orientation of the solar still is recommended for the location of Merida, Mexico. Taking this into consideration, all the subsequent experiments were carried out for the North-South orientation, reported in the following sections.

4.2. Influence of water depth on the performance of the solar still

Fig. 7 presents the hourly water temperature and coefficient of evaporation for three different water depths; 1, 2 and 3 cm, corresponding to 3, 6 and 9 L, respectively; with similar operating conditions, that is, solar irradiance: 820 W/m^2, wind speed: 2.5 m/s with predominant East-Southeast direction, relative humidity: 70%, dew point: 22°C and ambient temperature: 34°C. For better accuracy of the experiment, a gravity water flow was implemented to keep a constant basin water level during each evaluation.

In Fig. 7a, it is reported that higher water temperatures are obtained for lower water depths, observing that at 1,400 the following temperatures are obtained: 70.9°C for 1 cm of water depth, 68.3°C for 2 cm of water depth and 66.2°C for 3 cm of water depth. This phenomenon is observed because

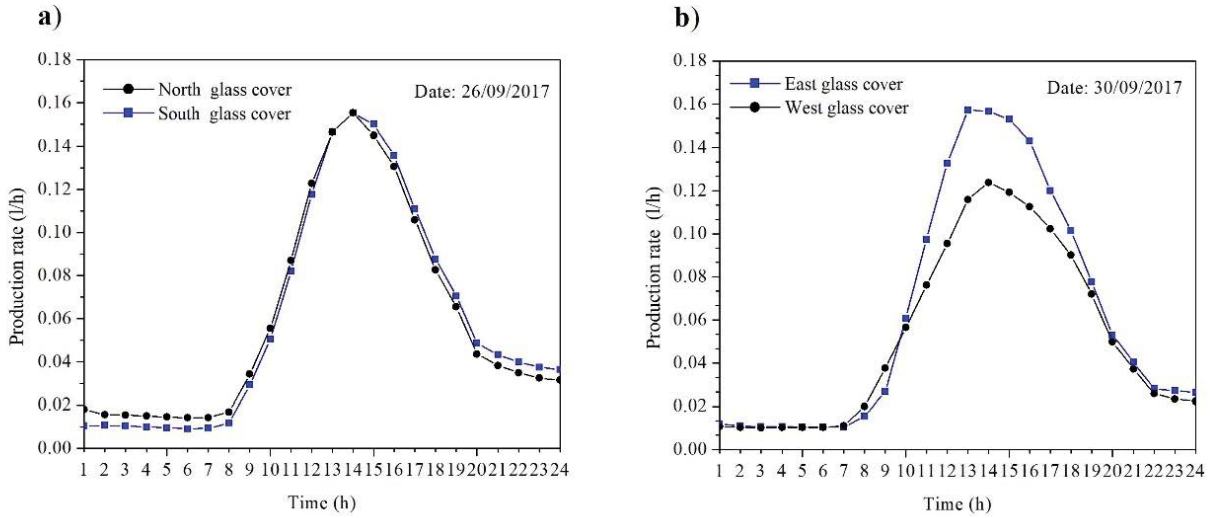

Fig. 6. Distillate water production rate for the solar still in (a) North-South orientation and (b) East-West orientation.

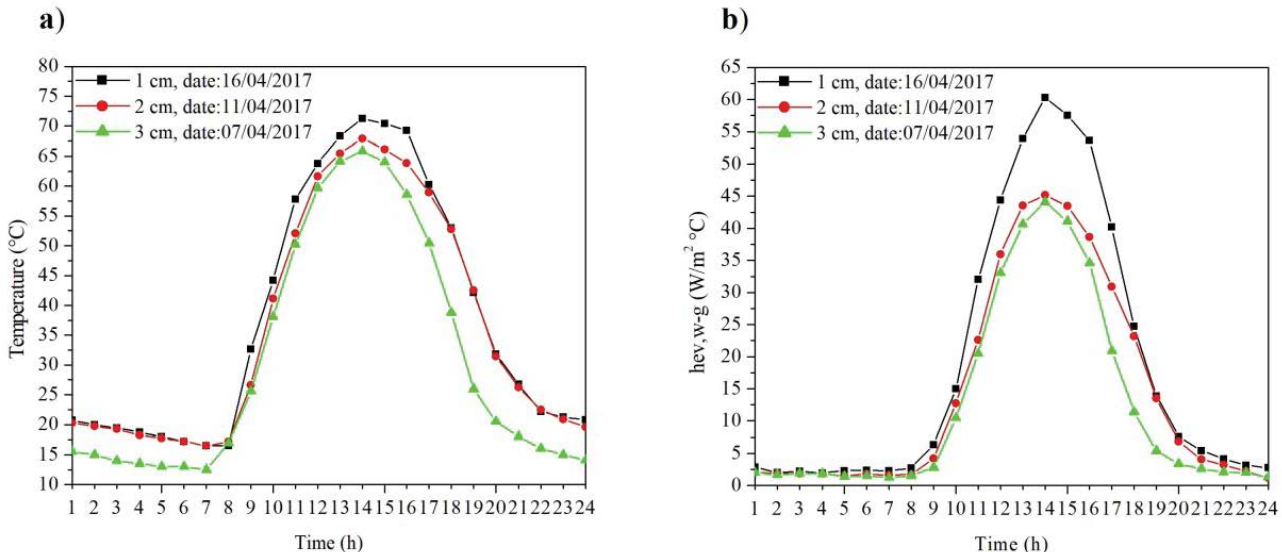

Fig. 7. Evaluation of the solar still at different basin water depths, (a) water temperature and (b) coefficient of evaporation.

the heat flux is inversely proportional to the mass content of the water. Additionally, the mass of the water is related to its heat capacity; therefore, it allows a rapid elevation in the water temperature (with less water). For example; a temperature of 35°C is achieved at 08:58 am for a water height of 1 cm, requiring 116.34 kJ of energy; the same temperature is achieved at 09:26 am for a water height of 2 cm, requiring 232.58 kJ of energy; and the same temperature is achieved at 09:35 am for a water height of 3 cm, requiring a total of 349.02 kJ of energy. In other words, the increment in the water depth requires more solar time for water evaporation purposes. Additionally, the evaporation coefficient calculated from Eq. (18) is presented in Fig. 7b, where it is observed that this coefficient increases as the basin water depth decreases, given that it is volumetric heat capacity also decreases; therefore, the thermal heat transfer is more effective as it is capable of accumulating more energy to overcome the intermolecular water forces. The highest evaporation coefficients are presented at 1,400 h, with 60.28, 45.14 and 44.06 W/m²°C, corresponding to 1, 2 and 3 cm depth, respectively.

Fig. 8 shows the production obtained for each water depth in the solar still, presented in terms of daily water productivity rate for the still area of 0.4 m² and its normalization to 1.0 m². Fig. 8a shows that the water production in the morning for the water depths of 1, 2 and 3 cm were 1.21, 1.08 and 0.75 l/h representing 88.39%, 84.28% and 70.88% of daily production, respectively. At lower water depths, higher temperatures were reached, which favors water evaporation. In contrast, during hours absent of solar energy (usually after 1,800 h) the water production for depths 1, 2 and 3 cm was 0.16, 0.20 and 0.31 l/h representing 11.61%, 15.72% and 29.17% of the daily production, respectively. This increase in nocturnal production for higher depths is due to the increase in the mass of water, which increases its heat capacity and

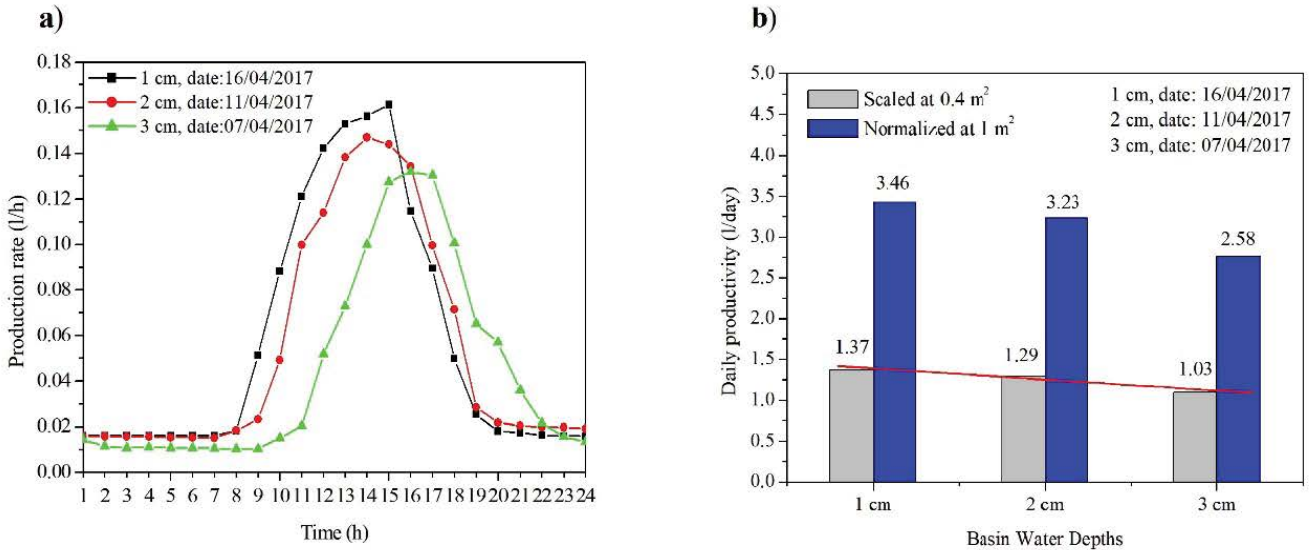

Fig. 8. Desalinated water daily production, (a) production rate at different depths in the basin and (b) daily productivity for scaled and normalized area.

causes the deeper water to cool more slowly and therefore results in greater water production.

The performance of the solar still is also presented in terms of the daily water productivity rate for the scaled area of 0.4 m² and a normalized area of 1.0 m² (Fig. 8b). It is possible to observe that, with an increase in water depth from 1 cm to 3 cm, the production reduces from 1.37 L/d (3.46 L/m² d) to 1.03 L/d (2.58 L/m² d); almost 25%, and with this, its efficiency; where this reduction is the consequence of the increase in the heat capacity of the water, confirming that the production is inversely proportional to the depth. Using Eq. (26), the average internal thermal efficiency for the depth of 1 cm was 32%, for 2 cm 30% and for 3 cm 24%. Rajamanickam and Ragupathy [16] reported that the maximum water productivity is at a water depth of 1 cm, which signifies that the current results comply with the results available in literature.

4.3. Time based thermal performance analysis of a solar still in Merida, Mexico

Figs. 9a and b show the daily-averaged monthly-distilled water production rate for a North-South orientation at 1 cm of water depth in the basin of distilled water production, with respect to the irradiance received and the efficiencies obtained during the year of operation, respectively.

In Fig. 9a it is possible to observe that the distillate production throughout the year follows the behavior of the

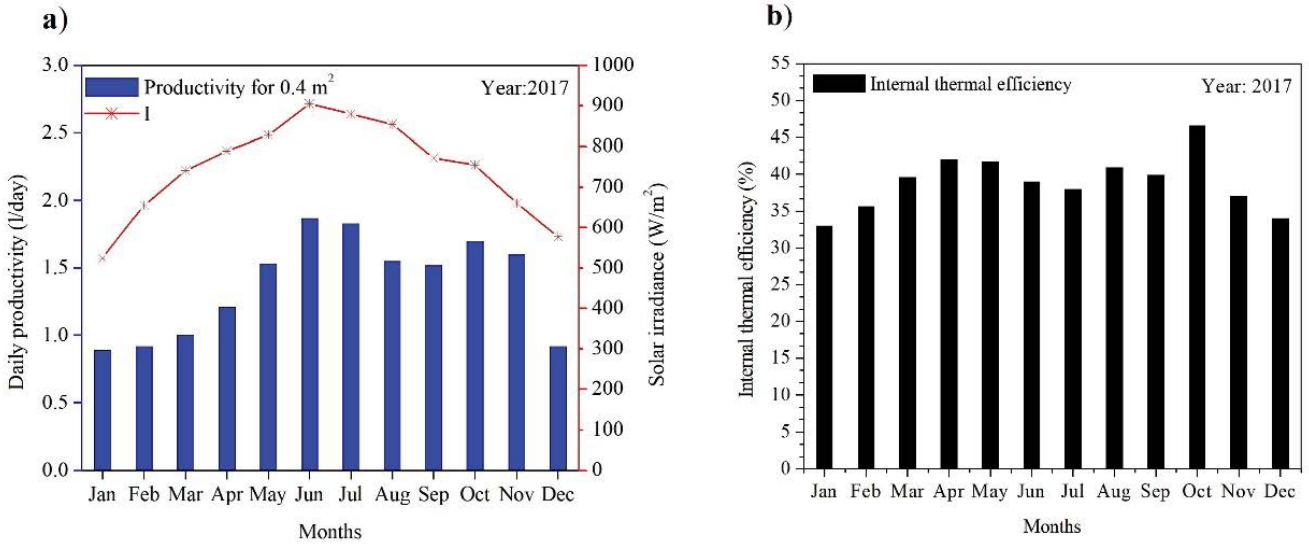

Fig. 9. Annual behavior of the solar still, (a) daily productivity per month and solar irradiance, scale 0.4 m² and (b) internal thermal efficiency of the system.

contributions of solar energy, corresponding to the typical sun's trajectory curve, with the maximum daily average in June of 1.88 L/d (4.69 L/m² d) with 905 W/m² and the minimum in January of 0.89 L/d (2.09 L/m² d) with 524 W/m². However, in some months, exceptions are observed which highlight the importance of the environmental factors that interact with the still system. This is particularly evident in October, when the efficiency increases with relatively low values of irradiance. This can be explained in terms of environmental factors, in which a combination of ambient cooler temperature and high winds during that month were favorable conditions for water condensation; highlighting the importance of the environmental factors interacting with the still system. For the month of July and August, a marked reduction in solar radiation can also be observed, resulting in a reduced distillate production because these months are cloudy at the study site. Table 1 shows the average daily production in seasonal terms related to the environmental parameters characteristic of each period. It can be seen that the highest production is in summer and the lowest is in winter, which aligned with the solar energy availability. However, autumn presents a higher production than spring despite having a lower energy input. This may be influenced by the lower ambient temperature (and wind) in autumn which generates a greater temperature differential between the glass cover and the still ambient (with vapor saturation), promoting more water condensation on the inner glass surface.

Fig. 9b shows the efficiency of the system during the study period, where it can be observed that the monthly averages of efficiency range between 33% and 46.56% with a maximum in October and a minimum in January. The average efficiency in the summer was 39.81% and 34.21% in winter. The average daily production for the year was 1.36 L/d (3.44 l/m² d) at an efficiency of 39.53% with 758 W/m². The results are presented in Table 2 for a solar still of 0.4 m², its normalized value at 1 m² and its respective internal thermal efficiency.

Fig. 10 shows the average daily production for the month of January and June, respectively, which presents a marked contrast in values during the period of study; with productivity minimums in the first case and productivity maximums in the second case.

In Fig. 10a we can observe that in January a minimum production of 0.11 L/d (0.27 L/m²·d) and a maximum of 1.27 L/d (3.17 L/m² d) was obtained, where the values of daily production were found to be very variable (standard deviation S = 0.37), due to the operating conditions characteristic of this month and the time range, with water temperatures above 35°C, from 900 to 1,700 h. In contrast, Fig. 10b shows that, for the month of June, a minimum production of 1.45 L/d (3.62 L/m² d) and a maximum of 2.18 L/d (5.45 L/m² d) were obtained, and the time range with water temperatures above 35°C was from 800 to 1,900 h; in addition, this month did not present significant differences in the daily production (S = 0.15), due to the fact that the solar irradiance is greater and the days are clearer. It is also important to note that some days of the month of January present high productions despite the lower average of solar irradiance in comparison with June, given that a day with greater solar irradiance or higher temperatures does not necessarily produce the highest quantity of distillate. In order for the

Table 1
Average daily production in seasonal terms

Season	Period	Ambient temperatura (°C)	Wind speed (m/s)	Solar irradiance (W/m²)	Production in litres (scaled at 0.4 m²)
Spring	March 1 to May 31	33.83	2.81	786	1.25
Summer	June 1 to August 31	34.30	2.35	880	1.75
Autumn	September 1 to November 30	31.47	2.28	729	1.58
Winter	December 1 to February 28	29.35	2.39	586	0.91

Table 2
Results obtained in the year of study

Results	Production in litres (scale of 0.4 m²)	Production in litres (Normalized at 1 m²)	Internal thermal efficiency (%)
Daily average per year	1.36	3.44	39.53
Maximum daily average per month (June)	1.88	4.69	39
Minimum daily average per month (January)	0.89	2.09	33
Daily maximum obtained in the year (June 12)	2.18	5.46	35.5
Daily minimum obtained in the year (January 10)	0.11	0.27	27.24
Average productivity in the Spring	1.25	3.12	41.12
Average productivity in the Summer	1.75	4.48	39.81
Average productivity in the Autumn	1.58	3.96	41.15
Average productivity in the Winter	0.91	2.28	34.21

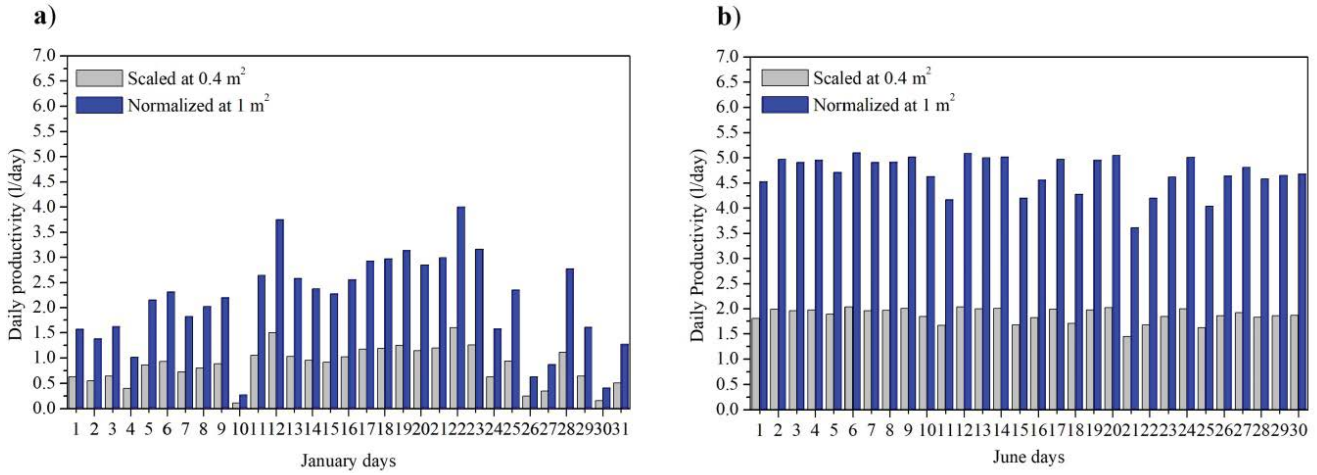

Fig. 10. Daily water productivity of the solar still, (a) January and (b) June.

condensation of water vapor to occur, there must be ambient conditions, which are favorable for the solar still, such as low ambient temperatures, low humidity levels and high wind speeds, which cool the glass covers.

Fig. 11 shows the behavior of the hourly temperatures in the most important parts of the solar still and the productivity, corresponding to the day with the highest production in the year (12 June 2017, North-South orientation with a water depth of 1 cm in the basin). Fig. 11a shows that the differences observed between the temperatures in the morning and those in the afternoon in each part of the solar still follow the behavior of the solar irradiance, even though the variations in the temperatures throughout the day appear delayed in time due to the thermal inertia of both; the materials and the system. In the morning, as the solar irradiance increases, the temperatures in the system also increased and, between 700 and 1,000 h, most of the heat gained is used to heat the water, while maintaining throughout this period a higher temperature, with respect to the basin, of almost 1.10%. During the subsequent hours, it is now the basin which acquires a higher temperature with respect to the water by 1.72%, representing a small difference because the water level is at 1 cm. The highest values of solar irradiance are observed between 900 and 1,500 h with a maximum at approximately 1200–1,300 h with 930 W/m^2. As the day continues, the temperature of the water and the basin reach their highest values and, as one would expect, the latter acquires the highest temperature since aluminum has the highest coefficient of thermal conductivity, with respect to the other materials employed; thus increasing the heat transfer rate to the system. For this day in particular, the average daytime temperature of the basin is 57.85°C, in the water it is 57.19°C, on the glass covers 46.35°C, the ambient air 35.87°C, with solar irradiance of 915 W/m^2; where the operating time for temperatures above 35°C in the water is between 800 and 1,900 h.

In Fig. 11a three very important behaviors can also be observed, the first one at 1,300 h presents the highest temperature difference between the glass covers (58.22°C) and the ambient air (37.92°C), a difference of 20.30°C, while the water reaches 71.64°C. The second one at 1,400 h presents the highest temperatures in the system, reaching the glass

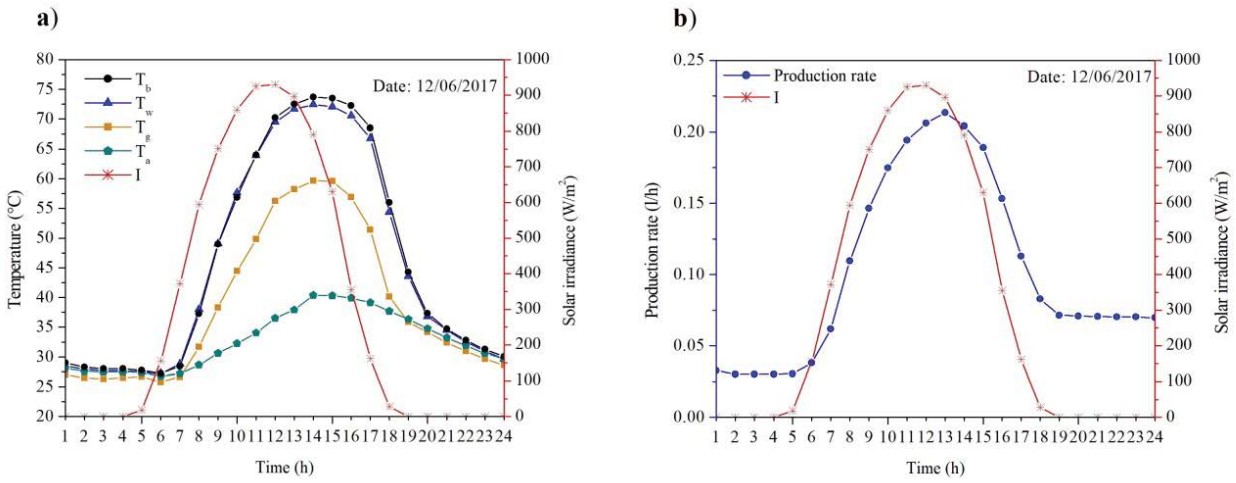

Fig. 11. Thermal response of the solar still, (a) temperature on different parts and (b) distilled water production.

covers at 59.64°C, in the water at 72.41°C and the ambient air at 40.38°C. The third one at 1,700 h presenting the greatest temperature difference between the water (66.77°C) and the glass covers (51.44°C) the difference being 15.33°C, where the ambient air was 39.14°C.

The behavior of the distilled water is presented with respect to the time of the day in Fig. 11b, where the production rate of distilled water is calculated using Eq. (27). It is observed that the production rate is delayed in comparison with the insolation because of the effect of the thermal inertia of water; however, both parameters maintain a similar behavior because the production rate is directly dependent on the water temperature, which increases with higher solar insolation. However, when the highest temperature in the system or the highest temperature difference between the water and the glass covers is acquired, this does not mean that the highest production rate will necessarily be obtained. In Fig. 11b, it can be observed that at 1,300 h the production peak is presented where the ambient air temperature is lower than it is at 1,400 h (highest temperatures in the system) and the water is hotter than it is at 1,700 h (greater difference between the water and the glass covers). Moreover, it is exactly at this point that the highest temperature difference between the glass covers and the ambient air is obtained, demonstrating that the surrounding temperature plays an important role in the yield of the system.

4.4. Heat transfer characteristics of the solar still

The heat transfer equations presented in section 3 are utilized to present the thermal behavior of the solar still for June 12, 2017 (Fig. 12). The dominant heat flows in the solar still primarily by convection and radiation, from the glass covers to the internal still system, representing 41.15% of the total energy received; the main energy inlet. Environmental factors such as the wind and the ambient air temperature have a direct effect on the glass cooling by accelerating the condensation of water vapor. Second in importance is the heat flow used in the evaporation of the water, of approximately 31.04%, representing the useful heat and the third is

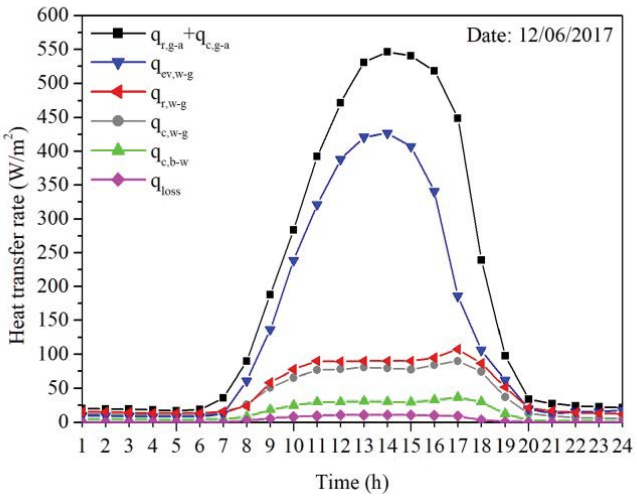

Fig. 12. Heat transfer characteristics of the solar still.

the heat by radiation of the water towards the glass covers of 11.07%, due to the emissivity between their surfaces.

The heat flow by convection from the water to the glass covers is linked to the quantity of internal air in the solar still which, due to considerations in the design, only represents 9.64% and it takes less time for the saturated vapor to reach the condensation surface by molecular diffusion. The heat flow by convection from the basin to the water is only 3.7%, reaffirming that the high transfer rate of heat to water is due to the radiative effects in conjunction with mass transfer. With respect to heat flow in the base of the solar still, it was found to be the lowest in the system with 1.26%, which can be considered negligible, confirming that the type and thickness of the insulation selected was adequate. Finally, the remaining 2.14% corresponds to heat loss due to leaks in the system.

4.5. Other important performance parameters of the solar still

In this section, the internal and the instantaneous thermal efficiency of the solar still is presented with respect to

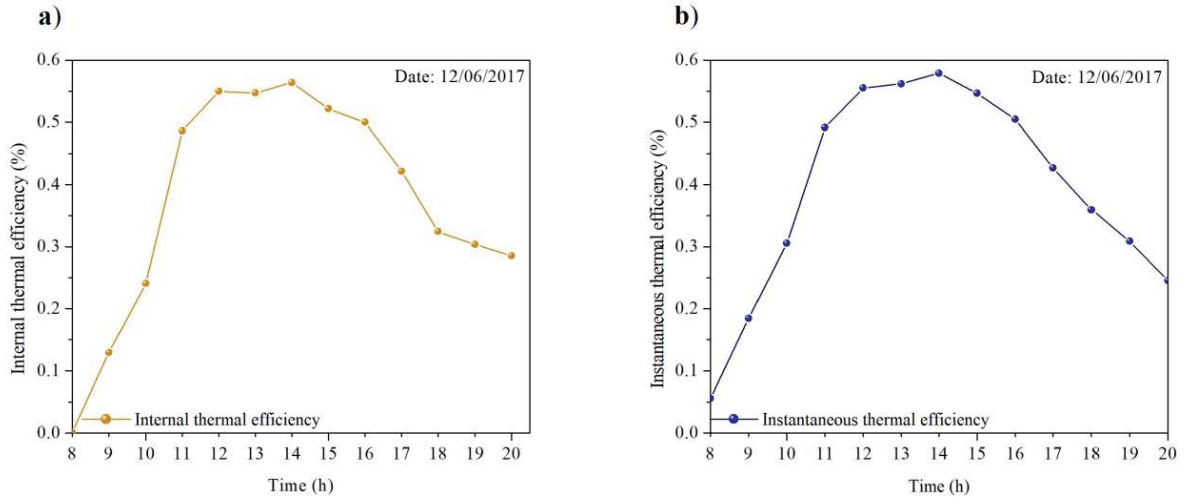

Fig. 13. Hourly thermal efficiency of the solar still, (a) internal and (b) instantaneous.

the time of the day (Fig. 13). It is observed that both of these performance parameters are dependent on the incident solar radiation; and they are also in a direct relationship with the operating temperatures of the solar still. For example, the internal thermal efficiency is maximum at 1,400 h at a value of ~54% (Fig. 13a); however, the average value is 35.5%. Similarly, the instantaneous thermal efficiency of the solar still also shows a trend similar to that of the water temperature (Fig. 13b), and it is also observed that the instantaneous efficiency reaches its peak for the highest water temperature; and afterwards it starts decreasing as the water temperature decreases. For example: a maximum instantaneous efficiency of ~58% is reported for 1,400 h, and the average instantaneous efficiency of ~39% is observed.

5. Cenote water quality analysis in Merida, Mexico

Table 3 presents the physicochemical and microbiological analyses of water samples from a cenote in Merida, Mexico, which is used by the inhabitants to satisfy their water needs (including its use as drinking water). This study was carried out before and after the water had been subjected to solar distillation and it was compared with the standard for drinking water of the World Health Organization 2011 (WHO-2011) [31].

The results presented in Table 3 shows that the water without treatment exceeds certain maximum permissible limits such as total hardness above 43.18% cataloged as very hard, electrical conductivity of 10%, dissolved solids 36.85% and high total alkalinity 89.88%. In addition, it presents an index of bacteriological contamination making it unfit for human consumption. It is also important to mention that some of the parameters exceed the average acceptable values, with a percentage of chlorides of 56.60% and ammonia at 60%. After subjecting the water to the process of distillation, high percentages of removal were obtained in the parameters mentioned above, resulting in soft water, free of salts and pathogenic agents; a water with 99% purity, suitable for human consumption.

6. Financial economics analysis

Table 4 shows the economical analysis of the project in terms of values to invest, costs and expenses using financial techniques such as the net present value (NPV), internal rate of return (IRR) and return of investment (ROI) [32]. In this case, the investment in the project are the costs of materials and the construction, the sum being US $166.36; the income is represented with US $159.19 from annual savings in the cost of buying purified water, taking into account the average daily production obtained; the expenses are the maintenance costs, including the operating costs; a total annual cost of US $36.23 and for this work the depreciation is defined in US $18.19, linear inflation of 5%, the salvage value of the system in 20%, the discount rate in 15% and the operating time as its average useful lifetime in 10 years [33].

The fact that the NPV is a positive value and higher than the initial investment indicates that it is convenient to carry out the project given that it provides economic savings to recover more than the invested amount. The IRR was higher

Table 3
Physicochemical and microbiological analysis of water before and after solar distillation under WHO-2011 standards for drinking water

No.	Water quality parameters	WHO maximum permissible levels (2011)	Before water treatment	Acceptable levels	After water treatment	Acceptable levels	Removal %	Units
1	Total coliforms	Absent	75	No	0	Yes	100	MPN/100 mL
2	Odor	Unobjectionable	Unobjectionable	Yes	Unobjectionable	Yes	–	NA
3	Color	Not exceeding 5 units	0	Yes	0	Yes	–	Hazen units
4	Taste	Unobjectionable	Unobjectionable	Yes	Unobjectionable	Yes	–	NA
5	Free residual chlorine	0.5–1.5	<0.1	Yes	<0.1	Yes	–	mg/L
6	Chloride	250	141.50	Yes	<1	Yes	99.29	mg/L
7	Total hardness	300	429.54	No	<2	Yes	99.53	mg/L
8	pH at 25°C	6.5–8.5	8.08	Yes	6.86	Yes	–	pH units
9	Electrical conductivity	100	110	No	0.8	Yes	99.27	ms/m
10	Nitrite	3	<0.01	Yes	<0.01	Yes	–	mg/L
11	Nitrate	50	2.43	Yes	<0.1	Yes	95.88	mg/L
12	Ammonia	0.5	<0.3	Yes	<0.3	Yes	–	mg/L
13	Total suspended solids	500	684.26	No	<5	Yes	99.27	mg/L
14	Sulphate	250	15.66	Yes	<0.5	Yes	96.81	mg/L
15	Total alkalinity	200	379.75	No	2.21	Yes	99.42	mg/L

Table 4
Economic analysis of the project

Annual period	Revenues	Expenses	Depreciation	Net cash flows	Accumulated without discount rate	Net flows NPV	Accumulated with discount rate
0	0	–166.36	–12.74	–179.10	–166.36	–166.36	–166.36
1	159.19	–36.23	–12.74	110.22	–56.14	95.85	–70.51
2	167.15	–38.04	–12.74	116.37	60.24	87.99	17.48
3	175.51	–39.94	–12.74	122.83	183.07	80.76	98.24
4	184.28	–41.94	–12.74	129.61	312.67	74.10	172.35
5	193.50	–44.04	–12.74	136.72	449.40	67.98	240.32
6	203.17	–46.24	–12.74	144.20	593.59	62.34	302.66
7	213.33	–48.55	–12.74	152.04	745.63	57.16	359.82
8	224.00	–50.98	–12.74	160.28	905.92	52.40	412.22
9	235.20	–53.53	–12.74	168.93	1,074.85	48.02	460.24
10	246.96	–56.20	–12.74	178.02	1,252.87	44.00	504.24

NPV	$491.51
IRR	66%
ROI	1.48
DROI	1.80

than the discount rate, confirming its viability since the rentability is higher than expected, and ROI with and without the discount rate is in 1.8 years (approximately 22 months) and 1.48 years (approximately 18 months), respectively.

7. Conclusions

In this work, a double slope solar still was developed to provide drinkable water alternatives for the peninsula of Yucatan, Mexico. The solar still was analyzed experimentally, and theoretically. The theoretical model was based on energy balance laws on different components of the solar still.

The following are the key findings:

- The North-South orientation of the solar still presented minor asymmetries in the thermal behavior of the glass covers, where the water reached higher temperatures and also a greater temperature difference between them, increasing the productivity by 14% with respect to the East-West orientation. It is reported that the temperature of the system is directly proportional to the solar irradiance and the water depth in the basin is inversely proportional to the production rate.
- The cyclical changes of the solar energy contributions affect the productivity of the solar still, which is 48% higher in the summer, in comparison with the winter. The highest, internal, thermal efficiency is obtained in the month of October with 46.5%, while the minimum is in January with 33%, due to the effect of diverse meteorological parameters and not just the high temperatures of operation characteristic, corresponding to the month of June.
- The highest production rates were obtained with the presence of maximum water temperature and the maximum temperature difference between the glass cover and the ambient air. The average daily production for the year was 1.36 L/d (3.44 L/m^2 d) with an efficiency of 39.73% at 758 W/m^2. The highest heat flows in the system are due to the convective and radiative effects from the glass covers to the ambient air of approximately 41.15%, followed by the evaporative effects of the water of 31.04% and the radiative effects between the water surface and the glass covers of 11.07%.
- From a financial point of view, the NPV has shown to be positive, thus it is a convenient project and the IRR is greater than the discount rate, demonstrating its rentability and the ROI in a short period of time, positioning the system as technically viable and economically affordable. The analysis of the water quality obtained shows that the process of solar distillation is effective in the removal of total coliforms, solids, salts and other elements with an efficiency of up to 99%, demonstrating that it is a good method of disinfection and procurement of water for human consumption, under the climate conditions of Merida, Mexico.

Acknowledgment

This work was supported by the project SENER-CONACYT S0019-2014-01 [grant number 254667] and the project PDCPN-CONACYT 2015-01 [grant number 1651]. The authors would like to thank the technical support from Francisco Koh-Dzul.

Symbols

T	—	Temperature, °C
k	—	Thermal conductivity coefficient, W/(m^2 °C)
v	—	Wind speed, m/s
P	—	Partial pressure, N/(m^2)
q	—	Heat transfer, W/(m^2)
q_{loss}	—	Heat loss from basin to ambient air, W/(m^2)
h	—	Heat transfer coefficient, W/(m^2 °C)
U_b	—	Overall heat loss coefficient from basin to ambient air, W/(m^2 °C)
I	—	Total solar irradiance, W/(m^2)
I'	—	Fraction of solar energy absorbed directly, W/(m^2)
q'	—	Energy balance, W/(m^2)

q_T — Total energy balance in the system, W/(m^2)
m — Mass, kg
L — Specific length, m
Ra — Rayleigh number, dimensionless

Greek

σ — Stefan-Boltzmann constant, W/(m^2 K^4)
λ — Latent heat, kJ/kg
δ — Thickness, m
η — Efficiency, %
ρ — Reflectance, dimensionless
α — Absorptance, dimensionless
ε — Emissivity, dimensionless

Subscripts

w — Water
g — Glass cover
b — Basin
a — Ambient air
s — Sky
r — Radiation
c — Convection
ev — Evaporative
i — Insulation
T — Total
int — Internal
ins — Instantaneous
eff — Effective

References

[1] A. Lysakowska, The Best Cenotes in Mexico: Ultimate Guide, Anna Everywhere, 2016, Available at: http://annaeverywhere.com/best-cenotes-tulum/, Accessed 9 Aug 2018.
[2] R. Tariq, N.A. Sheikh, J. Xamán, A. Bassam, An innovative air saturator for humidification-dehumidification desalination application, Appl. Energy, 228 (2018) 789–807.
[3] A. Kaushal, Varun, Solar stills: a review, Renewable Sustainable Energy Rev., 14 (2010) 446–453.
[4] L. Malaeb, K. Aboughali, G.M. Ayoub, Modeling of a modified solar still system with enhanced productivity, Sol. Energy, 125 (2016) 360–372.
[5] A. Aguilar, F. Bautista, M.E. Mendoza, O. Frausto, T. Ihl, Density of karst depressions in Yucatan state, Mexico, J. Cave Karst Stud., 78 (2016) 51–60.
[6] S. Rashidi, M. Bovand, N. Rahbar, J.A. Esfahani, Steps optimization and productivity enhancement in a nanofluid cascade solar still, Renewable Energy, 118 (2018) 536–545.
[7] V. Sivakumar, E. Ganapathy Sundaram, Improvement techniques of solar still efficiency: a review, Renewable Sustainable Energy Rev., 28 (2013) 246–264.
[8] J.C. Torchia-Núñez, M.A. Porta-Gándara, J.G. Cervantes-de Gortari, Exergy analysis of a passive solar still, Renewable Energy, 33 (2008) 608–616.
[9] W.M. El-Maghlany, An approach to optimization of double slope solar still geometry for maximum collected solar energy, Alexandria Eng. J., 54 (2015) 823–828.
[10] K. Kalidasa Murugavel, K. Srithar, Performance study on basin type double slope solar still with different wick materials and minimum mass of water, Renewable Energy, 36 (2011) 612–620.
[11] T. Rajaseenivasan, T. Elango, K. Kalidasa Murugavel, Comparative study of double basin and single basin solar stills, Desalination, 309 (2013) 27–31.
[12] V.K. Dwivedi, G.N. Tiwari, Experimental validation of thermal model of a double slope active solar still under natural circulation mode, Desalination, 220 (2010) 49–55.
[13] T. Arunkumar, R. Velraj, D.C. Denkenberger, R. Sathyamurthy, K. Vinoth Kumar, A. Ahsan, Productivity enhancements of compound parabolic concentrator tubular solar stills, Renewable Energy, 88 (2016) 391–400.
[14] F.B. Ziabari, A.Z. Sharak, H. Moghadam, F.F. Tabrizi, Theoretical and experimental study of cascade solar stills, Sol. Energy, 90 (2013) 205–211.
[15] B.I. Ismail, Design and performance of a transportable hemispherical solar still, Renewable Energy, 34 (2009) 145–150.
[16] M.R. Rajamanickam, A. Ragupathy, Influence of water depth on internal heat and mass transfer in a double slope solar still, Energy Procedia, 14 (2012) 1701–1708.
[17] A. Abdessemed, C. Bougriou, D. Guerraiche, R. Abachi, Effects of tray shape of a multi-stage solar still coupled to a parabolic concentrating solar collector in Algeria, Renewable Energy, 132 (2019) 1134–1140.
[18] M.S. Yousef, H. Hassan, M. Ahmed, S. Ookawara, Energy and exergy analysis of single slope passive solar still under Egyptian climate conditions, Energy Procedia, 141 (2017) 18–23.
[19] A. Kr. Tiwari, A. Somwanshi, Techno-economic analysis of mini solar distillation plants integrated with reservoir of garden fountain for hot and dry climate of Jodhpur (India), Sol. Energy, 160 (2018) 216–224.
[20] A.F. Mashaly, A.A. Alazba, Thermal performance analysis of an inclined passive solar still using agricultural drainage water and artificial neural network in arid climate, Sol. Energy, 153 (2017) 383–395.
[21] A.J.N. Khalifa, A.M. Hamood, On the verification of the effect of water depth on the performance of basin type solar stills, Sol. Energy, 83 (2009) 1312–1321.
[22] T. Elango, K.K. Murugavel, The effect of the water depth on the productivity for single and double basin double slope glass solar stills, Desalination, 359 (2015) 82–91.
[23] H. Taghvaei, H. Taghvaei, K. Jafarpur, M. Feilizadeh, M.R. Karimi Estahbanati., Experimental evaluation of the effect of solar collecting area on the performance of active solar stills with different brine depths, Desalination, 358 (2015) 76–83.
[24] M. Feilizadeh, M.R. Karimi Estahbanati, A. Ahsan, K. Jafarpur, A. Mersaghian, Effects of water and basin depths in single basin solar stills: an experimental and theoretical study, Energy Convers. Manage., 122 (2016) 174–181.
[25] S. Yadav, K. Sudhakar, Different domestic designs of solar stills: a review, Renewable Sustainable Energy Rev., 47 (2015) 718–731.
[26] M. Edalatpour, A. Kianifar, S. Ghiami, Effect of blade installation on heat transfer and fluid flow within a single slope solar still, Int. Commun. Heat Mass Transfer, 66 (2015) 63–70.
[27] M.M. Morad, H.A.M. El-Maghawry, K.I. Wasfy, Improving the double slope solar still performance by using flat-plate solar collector and cooling glass cover, Desalination, 373 (2015) 1–9.
[28] Z. Chen, J.T. Peng, G. Chen, L. Hou, T. Yu, Y. Yao, H.F. Zheng, Analysis of heat and mass transferring mechanism of multi-stage stacked-tray solar seawater desalination still and experimental research on its performance, Sol. Energy, 142 (2017) 278–287.
[29] S.A. El-Agouz, Y.A.F. El-Samadony, A.E. Kabeel, Performance evaluation of a continuous flow inclined solar still desalination system, Energy Convers. Manage., 101 (2015) 606–615.
[30] C. Elango, N. Gunasekaran, K. Sampathkumar, Thermal models of solar still—a comprehensive review, Renewable Sustainable Energy Rev., 47 (2015) 856–911.
[31] WHO, Guidelines for Drinking-Water Quality, World Health Organization, Fourth Edition, ISBN: 978-92-4-154995-0, 2017.
[32] E. Bas, A robust approach to the decision rules of NPV and IRR for simple projects, Appl. Math. Comput., 219 (2013) 5901–5908.
[33] A.E. Kabeel, A.M. Hamed, S.A. El-Agouz, Cost analysis of different solar still configurations, Energy, 365 (2010) 2901–2908.